Hindawi
Mathematical Problems in Engineering
Volume 2019, Article ID 7451967, 19 pages
https://doi.org/10.1155/2019/7451967

Research Article

Analysis of Heat Transfer in a Triangular Enclosure Filled with a Porous Medium Saturated with Magnetized Nanofluid Charged by an Exothermic Chemical Reaction

Raees-ul-Haq Muhammad

School of Mathematical Sciences, Shanghai Jiao Tong University, Shanghai 200240, China

Correspondence should be addressed to Raees-ul-Haq Muhammad; jdfortune@sjtu.edu.cn

Received 15 August 2019; Accepted 17 October 2019; Published 6 December 2019

Academic Editor: Alessandro Mauro

This paper intends to numerically study the steady-state free convection heat transfer in the presence of an exothermal chemical reaction governed by Arrhenius kinetics within a right-angled enclosure of triangular shape filled by porous media saturated with magnetized nanofluid. An approximation named as Darcy–Boussinesq approximation along with a nanofluid model mathematically propounded by Buongiorno has been implemented to model physical phenomenon representing fluid flow, heat transfer, and nanoparticle concentration. The mathematical equations in a dimensionless form describing the stream function for circulation of the fluid, the energy equation for heat, and nanoparticle volume fraction for concentration are solved using the finite difference method. The validity of the numerical procedure is established by comparing present results with the formerly available works in both statistical and graphical approaches. Streamlines, isotherms, and isoconcentrations are plotted and discussed for the various parametric regimes. The graphical description depicts that the average Nusselt and Sherwood numbers are the decreasing function of the Rayleigh number. The study revealed the accountable influence of model parameters such as thermophoresis and Brownian diffusion on the local Sherwood number, whereas a minimum impact on the local Nusselt number is observed.

1. Introduction

The flow of fluid and transfer of heat in a cavity filled by a nanofluid saturated with porous media are of vital importance in numerous practical situations. Some of these applications include geophysical applications, chemical reactors, building heating and cooling operations, electronic cooling equipment, and so on. Convective flows are studied extensively in enclosures filled with porous media as accounted in books by Pop and Ingham [1] and Bear [2]. Similarly, the enclosure of various geometric shapes is an essential aspect in engineering applications such as boilers or ovens with porous materials. Baytas and Pop [3] investigated the heat transfer characteristics for a steady-state flow in an inclined cavity filled with a porous medium. Sun and Pop [4] studied free convection in a triangular region filled with a porous medium. In their study, they placed a finite size flush mounted heater on the vertical wall of the cavity. They concluded that the average Nusselt number has a maximum value with a smaller aspect ratio of enclosure dimensions. It also has a lesser value by the lowest position of the heater with the highest magnitude of Rayleigh number and the maximum size of the heater. Izadi et al. [5] performed a numerical investigation of the natural convection heat transfer of a hybrid nanofluid into a porous cavity exposed to a variable magnetic field. Their findings indicate that at higher Rayleigh number, by increasing the Hartmann number, a significant decrease in Nusselt number occurs, which can be attributed to the decreased power of the flow. Arpino et al. [6] studied unsteady free convection in a partially porous annular enclosure and employed an adaptive local time-stepping procedure based

on a properly stabilized full matrix-inversion scheme. They concluded that the position of the porous layer in the annulus strongly affected the stability of the free convection. Arpino et al. [7] have also studied porous medium-free fluid interface problems in the presence of high source terms by using a stable, accurate, and efficient artificial compressibility (AC) characteristic-based split (CBS) algorithm. In another paper, Arpindo et al. [8] presented an efficient three-dimensional algorithm based on the fully explicit matrix-inversion free finite element version of the characteristic-based split (CBS) scheme. The scheme was applied for the first time to the simulation of complex thermo-fluid-dynamic problems in domains containing a fluid and a porous layer. Massaroti et al. [9] adopted a dual time-stepping procedure based on the transient artificial compressibility version of the characteristic-based split algorithm to solve the transient equations of the generalized model for heat and fluid flow through porous media. Shermet and Pop [10] also studied steady-state free convection heat transfer in a right-angle triangular cavity filled with a porous medium using the mathematical nanofluid model proposed by Buongiorno [11].

The subject of nanofluids has received considerable concentration from the researchers for its role in engineering and Biophysics fields. The presence of nanoscale particles in the fluid enhances heat transfer characteristics and has been used widely in the industry. For example, materials with sizes of nanometers possess unique physical and chemical properties (Oztop and Abu-Nada [12]). They tested Cu (copper), Al_2O_3 (alumina), and T_iO_2 (titania) as the base fluid to study the effect of nanoparticles on natural convection and thermal profiles. Choi [13] first introduced the term nanofluid which rooted from the addition of nanoscale particles to the fluids. The presence of nanoparticles in the fluid enhances the thermal conductivity within it. In a recent catalogue of articles by Kuznetsov and Nield [14] and Nield and Kuznetsov [15], a lot more have implemented Buongiorno's mathematical model for nanofluids to study problems on Newtonian fluids and porous media filled by nanofluids. The authors reported that the use of surfactant or surface charge technology could cause suspension of nanoparticles in the nanofluid, hence preventing the particles from deposition on the porous matrix. Nanofluids have vital importance in the areas involving solar collectors to absorb solar thermal radiations. A wide set of nanofluid applications is recently reported in the books by Nield and Bejan [16] and YuS et al. [17]. Among several nanofluid mathematical models, Buongiorno's model [11] received considerable attention since he noted that the effect of the velocity between nanoparticles and base fluids. Also, he has written down the conservation equations considering the two important effects which are the Brownian diffusion and the thermophoresis effects.

The area of fluid mechanics that investigates the characteristics of fluids with electrical conductivity in the presence of an electromagnetic field is known as Magnetohydrodynamics (MHD). MHD convection flow has a wide range of applications in the area of science and engineering. These include geothermal energy extractions, petroleum reservoirs thermal insulation, plasma confinement, crystal growth, and nuclear reactor coolers. Chamkha [18] investigated the hydrodynamic convection flow in a vertical lid-driven cavity with absorption or internal heat generation. Malleswaram and Sivasankaran [19] presented a numerical analysis on magnetohydrodynamic-mixed convection in a lid-driven cavity when both the side-walls are provided with nonuniform heating. AlimM et al. [20] have presented a numerical study for the conjugate effect of Joule heating and MHD-mixed convection in a lid-driven square cavity. Rahman et al. [21] also studied the free convection within a tilted cavity filled with nanofluid in the presence of a porous medium and a sloping magnetic field energized by an exothermic chemical reaction. They concluded that the presence of the magnetic field causes the nanoparticles to separate from the fluid with small velocity. The process of free convection in the presence of an exothermic surface reaction has widely been studied by Merkin and Chaudhary [22], Mahmood and Merkin [23], Ikeda et al. [24], Gray and Merkin [25, 26], and Merkin and Pop [27]. Single first-order kinetic equation with Arrhenius [28] thermal energy dependence models the reaction on the surface and is defined as

$$\begin{aligned} &A \longrightarrow B, \\ &\text{rate} = k_0 a e^{-(E/RT)}, \end{aligned} \tag{1}$$

where A and B are the reactants, k_0 denotes pre-exponential factor, a represents the reactant $A's$ concentration, and E and R represent the activation energy and fluid constant, respectively. Rahman [29] investigated a higher order chemical reaction along with internal heat generation on a non-Darcian forced convection for an incompressible viscous fluid flow with thermal conductivity across an elastic surface interlaced in a porous medium. He concluded that with the increase in Darcy number, the dynamic viscosity alongside the thermal conductivity reduces.

It is apparent from the preceding literature study that most of the reviews are performed considering the nanofluids in cavities, but very less attention is paid to study the cavities filled with the porous medium saturated with nanofluids particularly in the presence of MHD and chemical reaction. So, in this paper, we study free convection within a triangular cavity filled with porous media saturated with nanofluid using Buongiorno's model [11] incorporating Darcy's law for the flow in the porous medium. We also employed the Boussinesq approximation to model the governing equations for the convective forces. The resulting partial differential equations of the advection-diffusion type are solved numerically using a finite difference method. The description of the scheme is presented in Appendix. To the best of authors' knowledge, the problem of natural convection within a triangular cavity in the presence of a magnetic field driven by an exothermic chemical reaction using the mathematical nanofluid model has not been reported yet in the literature. As such, the focus of this paper is to study the detailed and attributed analysis on the flow and heat transfer due to the effects of pertinent parameters arising in the problem.

2. Problem Formulation

2.1. Physical Model. We consider an isosceles triangular-shaped cavity filled with a porous medium saturated with nanofluid consisting of water and nanoparticles. The $\overline{x}$-axis is along the bottom wall of width H, while the $\overline{y}$-axis is along the vertical wall of the cavity with length L and maintained at the constant temperature T_o and the constant nanoparticle volume fraction C_o. A similar assumption is also made for the inclined boundary, while the bottom wall along the $\overline{x}$-axis is assumed to be adiabatic. A magnetic field F_b with strength B_0 is imposed within the fluid along the positive x-axis. An exothermal surface reaction governed by Arrhenius kinetics [28] is also taken into account inside the cavity which is of order one and nonisothermal. Figure 1 represents the schematic diagram of problem geometry and the coordinate system. Water-based nanofluid inside the cavity is chosen for the analysis and is set to be laminar and incompressible. The base fluid (i.e., water) and the nanoparticles are assumed to be in thermal equilibrium. Hence, no slip occurs between them. The suspension of nanoparticles within the nanofluid is expected to be carried out using either surfactant or surface charge technology. Inside the triangular cavity, the fluid flow is considered to be weak, laminar, and incompressible with no heat transfer due to the viscous dissipation as well as the radiation. The nanofluid density depends on the volume fraction of nanoparticles and the temperature, while the other thermophysical properties of the nanofluid are expected to be constant. Compared to the initial temperature T_0, the increase in temperature inside the flow domain is assumed to be smaller. As reported by CardosoT et al. [30], the rise in temperature before a chemical reaction is approximately below $10-50$ K, while general consideration of initial temperature T_0 is below 632.2 K. Hence, the Darcy–Boussinesq approximation is adapted for the present problem.

2.2. Governing Equations. With the assumption that viscous dissipation effects are negligible, the Oberbeck–Boussinesq approximation is employed, and Darcy's law is applicable. By following the nanofluid model proposed by Buongiorno [11], the governing equations for total mass, momentum, energy, and nanoparticles, respectively, are written as

$$\begin{gathered}
\vec{\nabla}\cdot\vec{V}=0,\\
0=-\vec{\nabla}P^{*}-\frac{\mu}{K}\vec{V}+\vec{F}_b+\rho g\hat{j},\\
(\rho c)_f\vec{V}\cdot\vec{\nabla}T=k_m\vec{\nabla}^2T+\varepsilon(\rho c)_p\left[D_B\vec{\nabla}T\cdot\vec{\nabla}C\right.\\
\left.+\frac{D_T}{T_0}\vec{\nabla}T\cdot\vec{\nabla}T\right]+Qk_0ae^{-(E/RT)},\\
\frac{1}{\varepsilon}\vec{V}\cdot\vec{\nabla}C=D_B\vec{\nabla}^2C+\frac{D_T}{T_0}\vec{\nabla}^2T,
\end{gathered}\tag{2}$$

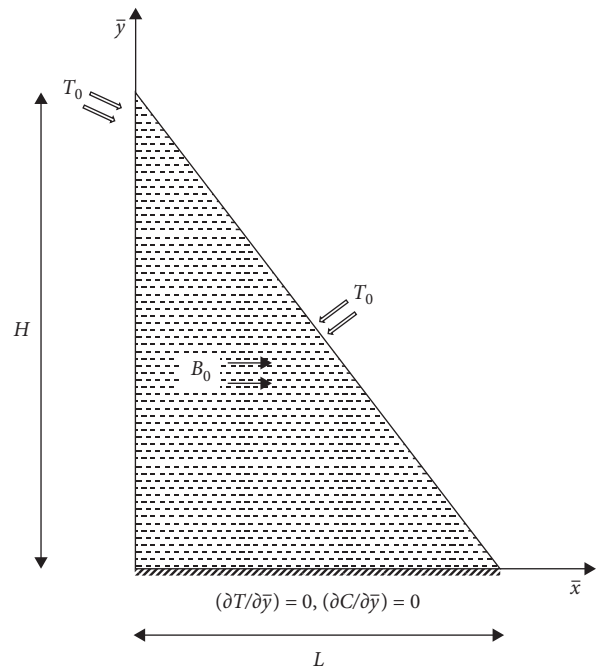

Figure 1: Problem geometry.

where $\vec{F_b}$ is given by $\vec{F_b}=\sigma(\vec{u}\times\vec{B})\times\vec{B}$, $\vec{B}=(B_0,0,0)$ is the constant magnetic field strength along $\overline{x}$–axis, and the buoyancy term $\rho\mathbf{g}$ is approximated by the Boussinesq approximation:

$$\rho\mathbf{g}=-\rho_{f_0}\beta(1-C_0)\frac{\partial T}{\partial\overline{x}}g+\left(\rho_p-\rho_{f_0}\right)\frac{\partial C}{\partial\overline{x}}g. \tag{3}$$

Here, $\vec{V}=(\overline{u},\overline{v},0)$ is the velocity vector with $\overline{u}$ and $\overline{v}$ the nanofluid velocity components along $\overline{x}$– and $\overline{y}$–axis, respectively, T is the nanofluid temperature, C is the nanoparticle volume fraction, and other quantities of physical interest are mentioned in Nomenclature. To nondimensionalize the governing equations along with boundary conditions, we make use of the following similarity transformations:

$$\begin{gathered}
x=\frac{\overline{x}}{H},\\
y=\frac{\overline{y}}{H},\\
u=\frac{H}{\alpha_m}\overline{u},\\
v=\frac{H}{\alpha_m}\overline{v},\\
\theta=\frac{E(T-T_0)}{RT_0^2},\\
\phi=\frac{C}{C_0},\\
P=\frac{P^{*}K}{\mu\alpha_m}.
\end{gathered}\tag{4}$$

Following the traditional way of defining the dimensionless stream function ψ from velocity components as follows:

$$\overline{u} = \frac{\partial \psi}{\partial \overline{y}}, \qquad \overline{v} = -\frac{\partial \psi}{\partial \overline{x}}. \tag{5}$$

Using the dimensionless variables defined in equation (4) and the stream function in equation (5), the governing equations now take the form:

$$\nabla^2 \psi + H_a^2 \frac{\partial^2 \psi}{\partial x^2} + R_a \frac{\partial \theta}{\partial x} - R_a N_r \frac{\partial \phi}{\partial x} = 0, \tag{6}$$

$$\nabla^2 \theta - \left(\frac{\partial \psi}{\partial y} \frac{\partial \theta}{\partial x} - \frac{\partial \psi}{\partial x} \frac{\partial \theta}{\partial y} \right) + N_b \left(\frac{\partial \phi}{\partial x} \frac{\partial \theta}{\partial x} + \frac{\partial \phi}{\partial y} \frac{\partial \theta}{\partial y} \right) + N_t \left[\left(\frac{\partial \theta}{\partial x} \right)^2 + \left(\frac{\partial \theta}{\partial y} \right)^2 \right] + F_k e^{\theta} = 0, \tag{7}$$

$$\nabla^2 \phi - L_e \left(\frac{\partial \psi}{\partial y} \frac{\partial \phi}{\partial x} - \frac{\partial \psi}{\partial x} \frac{\partial \phi}{\partial y} \right) + \frac{N_t}{N_b} \nabla^2 \theta = 0. \tag{8}$$

The boundary conditions are as follows:

$$\psi = 0, \quad \theta = 0, \quad \phi = 1, \quad \text{at } x = 0, \tag{9}$$

$$\psi = 0, \quad \theta = 0, \quad \phi = 1, \quad \text{at } x + y = 1, \tag{10}$$

$$\psi = 0, \quad \frac{\partial \theta}{\partial y} = 0, \quad \frac{\partial \phi}{\partial y} = 0, \quad \text{at } y = 0, \tag{11}$$

where H_a is the magnetic field parameter also known as the modified Hartmann number, R_a is the Rayleigh number, N_r is the buoyancy-ratio parameter, N_b is the Brownian motion parameter, N_t is the thermophoresis parameter, F_k is the Frank-Kamenetskii number, L_e is the Lewis number, and the Laplacian operator ∇^2 are all defined as

$$\begin{aligned} H_a &= \frac{\sigma B_0^2 K}{\mu}, \\ R_a &= \frac{(1 - C_0)\rho_{f_0} g \beta K R T_0^2 L}{\mu \alpha_m E}, \\ N_r &= \frac{(\rho_p - \rho_{f_0}) C_0 E}{\rho_{f_0} \beta (1 - C_0) R T_0^2}, \\ N_b &= \frac{\tau C_0 D_B}{\alpha_m}, \\ N_t &= \frac{\tau D_T R T_0}{\alpha_m E}, \\ F_k &= \frac{E Q k_0 a \exp(E/RT_0) L^2}{R T_0^2 \alpha_m}, \\ L_e &= \frac{\alpha_m}{\varepsilon D_B}, \\ \nabla^2 &= \frac{\partial^2}{\partial x^2} + \frac{\partial^2}{\partial y^2}. \end{aligned} \tag{12}$$

For problems related to heat and mass transfer across the cavity, it is essential to determine rates of heat and mass transfer in terms of local and average Nusselt and Sherwood numbers, respectively, using the following formulas:

$$\begin{aligned} N_u &= -\left(\frac{\partial \theta}{\partial x} \right)_{x=0}, \\ S_h &= -\left(\frac{\partial \phi}{\partial x} \right)_{x=0}, \\ \overline{N_u} &= \int_0^1 N_u \mathrm{d}y, \\ \overline{S_h} &= \int_0^1 S_h \mathrm{d}y. \end{aligned} \tag{13}$$

3. Numerical Method

We employ the finite difference method in combination with an iterative procedure [31] to solve the governing equations (6)–(8) along with boundary conditions (9). A five-point cell-centered stencil with a central difference formula is applied to obtain the system of linear equations which are then addressed in MATLAB. The step size is chosen to be uniform in both x and y directions. For the convergence criteria, 10^{-6} is chosen as a tolerance error for all dependent variables. The iterative procedure is terminated once the following convergence criteria are satisfied:

$$\frac{\sum_{i=1}^{M}\sum_{j=1}^{N}\left|\chi_{i,j}^{n+1}-\chi_{i,j}^{n}\right|}{\sum_{i=1}^{M}\sum_{j=1}^{N}\left|\chi_{i,j}^{n+1}\right|}\leq 10^{-6},\quad n\geq 1, \tag{14}$$

where χ represents the dependent variables ψ, θ or ϕ, while M and N are the number of grid points along x and y directions, respectively, and n is the iteration index.

3.1. Test for Grid Independence. For correct usage of the finite difference method, it is essential to perform grid sensitivity analysis on the converged solutions. Thus, eight cases of a uniform grid varying from 8×8 to 128×128 with an increment of 32×32 are tested. The numerical simulations for the grid independence test are shown for selected values of the model parameters $R_a = 10$, $H_a = 2$, $N_r = 0.1$, $N_b = N_t = 0.4$, $L_e = 1$, and $F_k = 0.1$. The test is conducted by plotting the average Nusselt number against the number of grid points. As can be seen in Figure 2, the value of the average Nusselt number almost becomes independent of grid size when the grid points are higher than 128×128. Hence, a regular grid of 128×128 points has been selected for the following analysis.

3.2. Corroboration of the Numerical Code. We performed graphical as well as statistical tests for the corroboration of a numerical code. One of the two tests compares the average Nusselt number ($\overline{N_u}$) for a regular fluid with different values of Rayleigh number $R_a = 10-10^4$. The results are reported in Table 1 for the parameters $N_t = N_r = N_b = 0$, $H_a = 0$, $L_e = 0$, and $F_k = 0$, which reduce the problem to one mentioned in references [3, 10, 32–37].

The second test is performed to compare the obtained results for streamlines, isotherms, and isoconcentrations with the numerical data of [10]. They have studied the steady free convection flow and heat transfer in a triangular enclosure filled with a porous medium which is of the same geometry as our problem. The numerical simulations are performed by setting $H_a = 0$ and $F_k = 0$, which reduce the present study to the reference problem. Figures 3 and 4 compare the present results with previous results and are approximately the same compared to those of Sheremet and Pop [10]. These tests for the comparison of results obtained for the present study and their agreement boost the confidence of the current numerical scheme.

4. Results and Discussion

This section discusses the numerical simulation results and presents the graphical results of streamlines, isotherms, isoconcentrations, and average Nusselt number and average Sherwood number for various model parameters in a triangular enclosure. The effects of different values of Rayleigh number ($R_a = 10-10^4$), modified Hartmann number ($H_a = 0-10$), Brownian motion parameter ($N_b = 0.1-0.4$), thermophoresis parameter ($N_t = 0.1-0.4$), buoyancy-ratio parameter ($N_r = 0.1-0.4$), Lewis number ($L_e = 1-10$), and Frank-Kamenetskii number ($F_k = 0.1-0.3$) on the flow and heat transfer characteristics are analyzed.

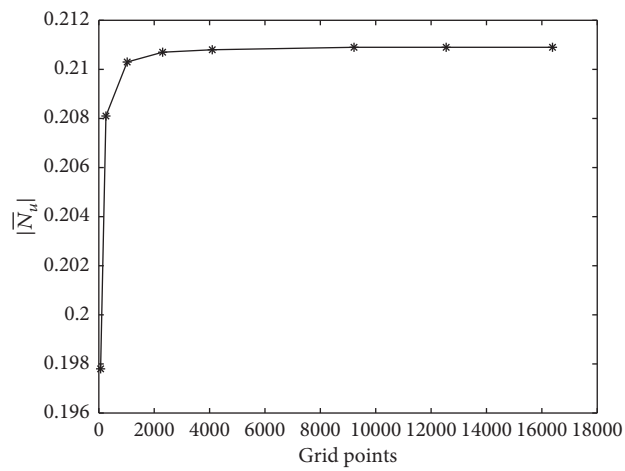

Figure 2: Average Nusselt number for different number of grid points.

Table 1: Average Nusselt number $\overline{N_u}$ for various values of R_a.

Previous results	R_a			
	10	100	1000	10000
Sheremet and Pop [10]	1.071	3.104	13.839	49.253
Walker and Homsy [32]	—	3.097	12.96	51.0
Bejan [33]	—	4.2	15.8	50.8
Beckermann et al. [34]	—	3.113	—	48.9
Gross et al. [35]	—	3.141	13.448	42.583
RamosS et al. [36]	1.065	2.801	—	—
Baytas and Pop [3]	1.079	3.16	14.06	48.33
Manole and Lage [37]	—	3.104	13.637	48.117
Present results	1.022	3.4	13.366	43.74

4.1. Explanation of Physical Parameters. It is useful to present the physical reasons for variation in each vital parameter. In fluid mechanics, Rayleigh number (R_a) is the property of a fluid that determines how heat is transferred throughout the fluid. The Rayleigh number is closely related to Grashof number (G_r), and both numbers are used to describe natural convection and heat transfer by natural convection. The Rayleigh number is simply defined as the product of the Grashof number, which represents the relationship between buoyancy and viscosity within a fluid, and the Prandtl number, which describes the relationship between momentum diffusivity and thermal diffusivity. A smaller value of Rayleigh number represents the laminar flow, while a higher range indicates a turbulent flow. The buoyancy-ratio parameter describes an effect of the buoyancy force due to the concentration difference in comparison with the buoyancy force due to temperature difference. N_b, the Brownian motion parameter describes the movement of nanoparticles and enlightens the thermal effects of the nanofluid and nanoparticle diameter, whereas the thermophoresis parameter N_t explains the temperature gradient effect on nanoparticle diffusion depending on the thermal conductivity of the fluid and particle materials. The Lewis number is a dimensionless number, named after Warren K. Lewis, defined as the ratio of thermal diffusivity

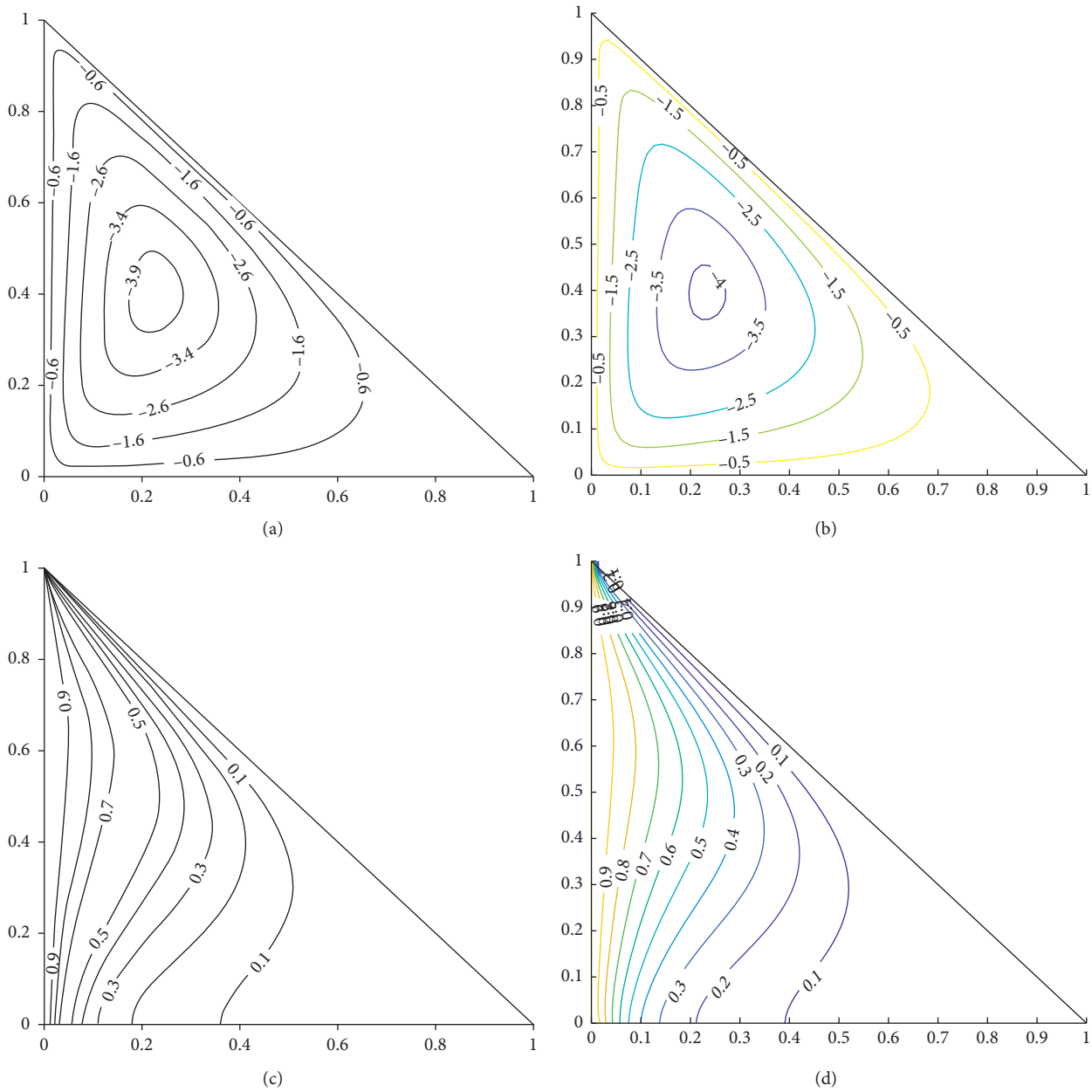

Figure 3: Continued.

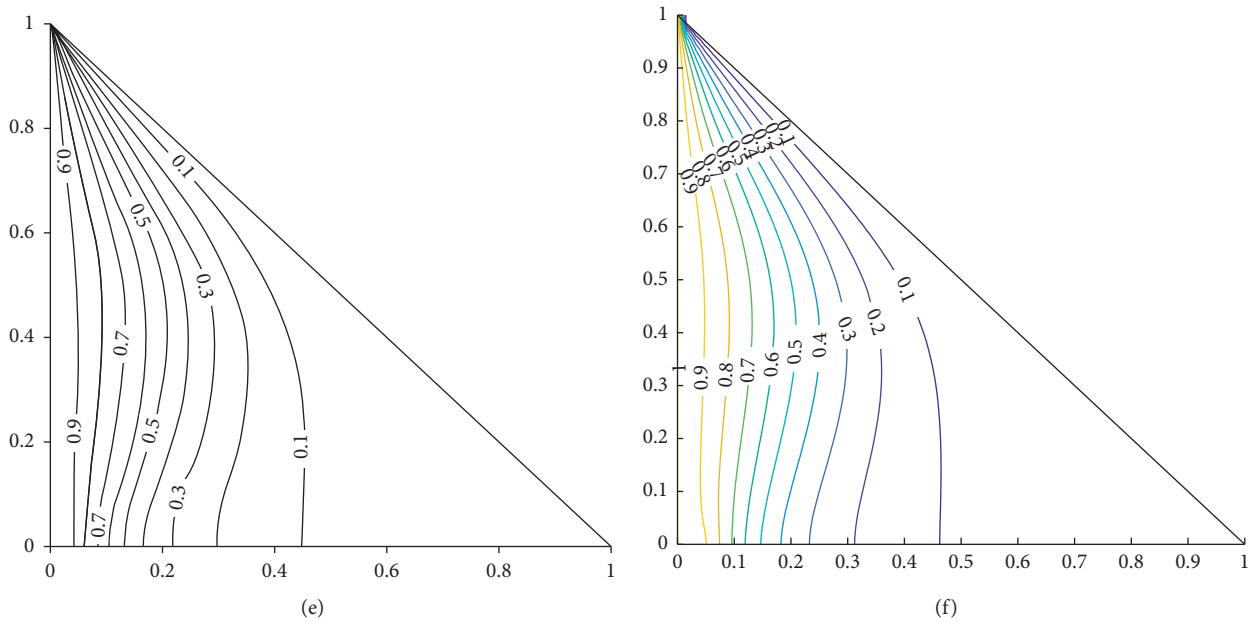

Figure 3: Comparison of results for $N_r = 0.1$, $N_b = 0.1$, and $N_t = 0.1$ when $R_a = 100$ and $L_e = 1.0$. (a) Streamlines ψ of Sheremet and Pop [10]. (b) Streamlines ψ of present results. (c) Isotherms θ of Sheremet and Pop [10]. (d) Isotherms θ of present results. (e) Isoconcentrations ϕ of Sheremet and Pop [10]. (f) Isoconcentrations ϕ of present results.

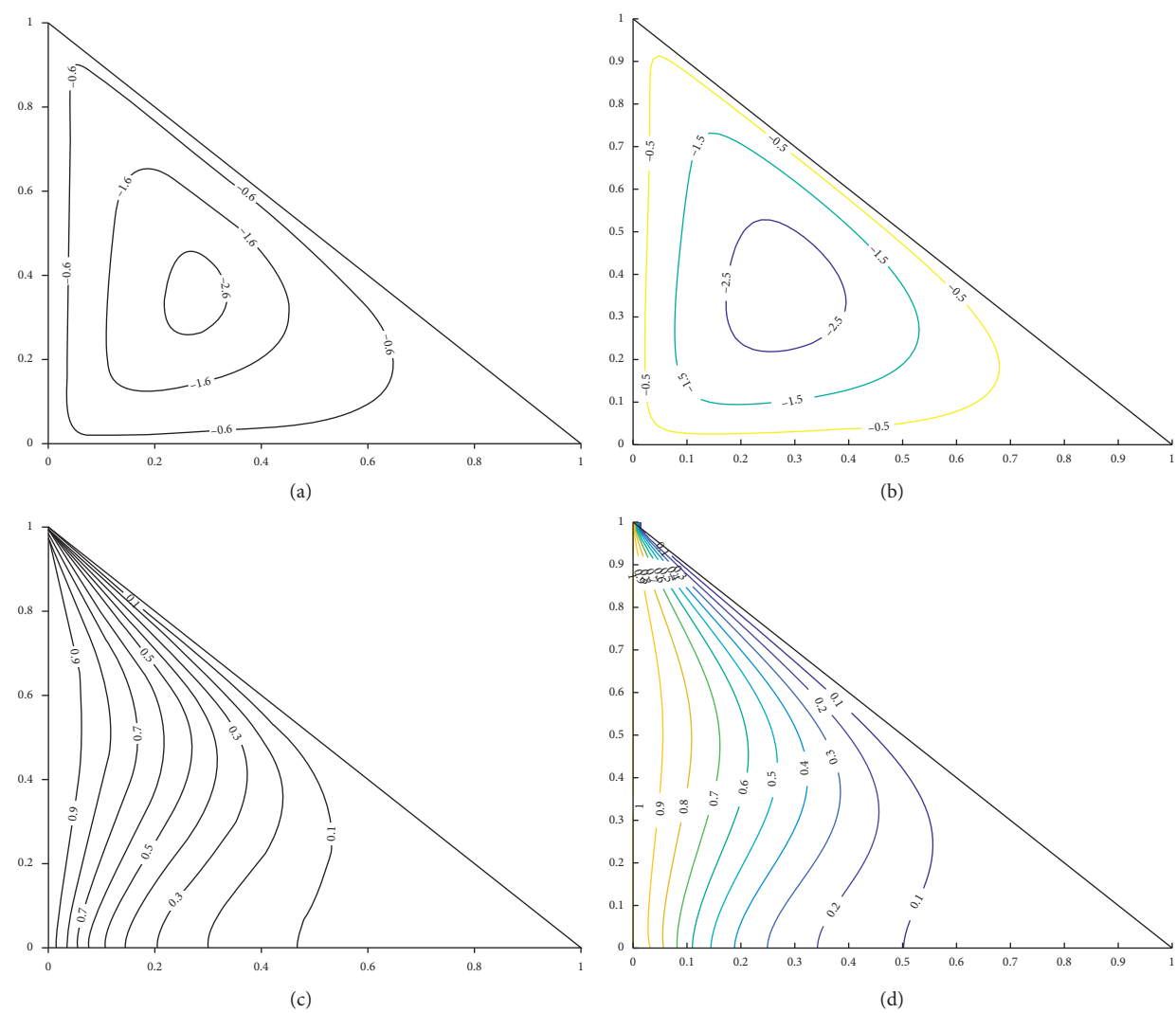

Figure 4: Continued.

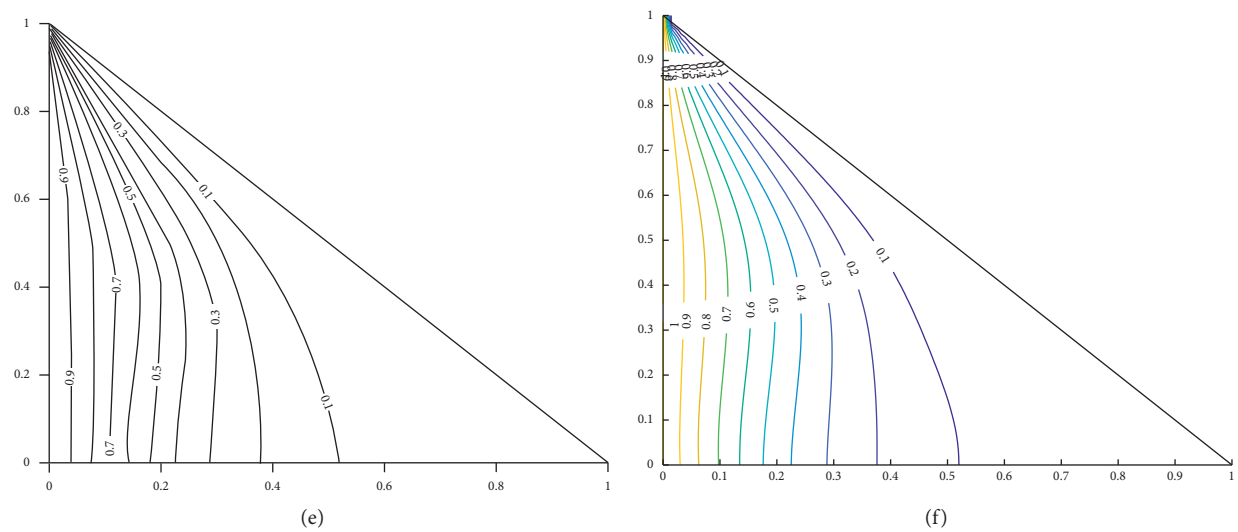

Figure 4: Comparison of results for $N_r = 0.4$, $N_b = 0.4$, and $N_t = 0.4$ when $R_a = 100$ and $L_e = 1.0$. (a) Streamlines ψ of Sheremet and Pop [10]. (b) Streamlines ψ of present results. (c) Isotherms θ of Sheremet and Pop [10]. (d) Isotherms θ of present results. (e) Isoconcentrations ϕ of Sheremet and Pop [10]. (f) Isoconcentrations ϕ of present results.

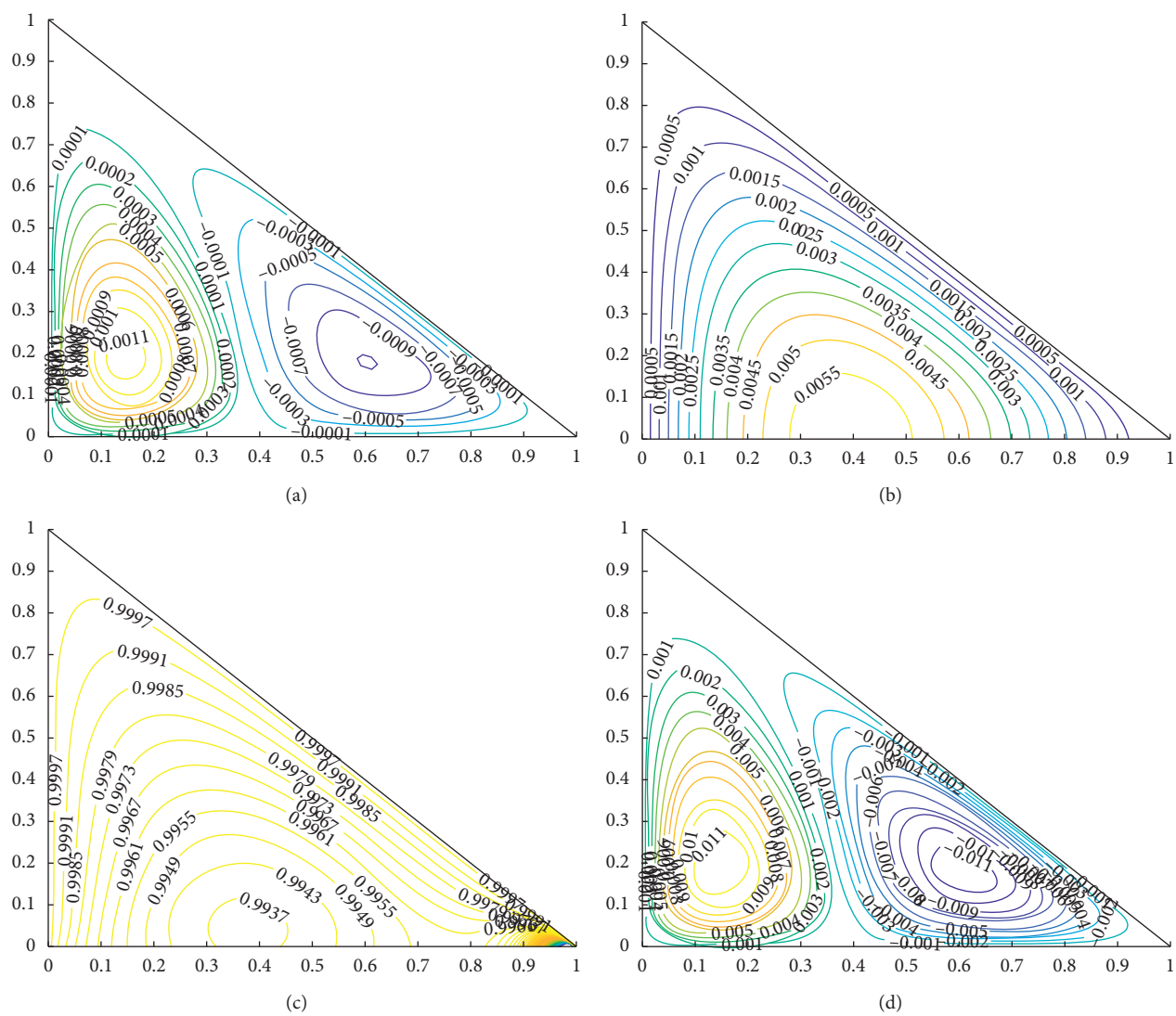

Figure 5: Continued.

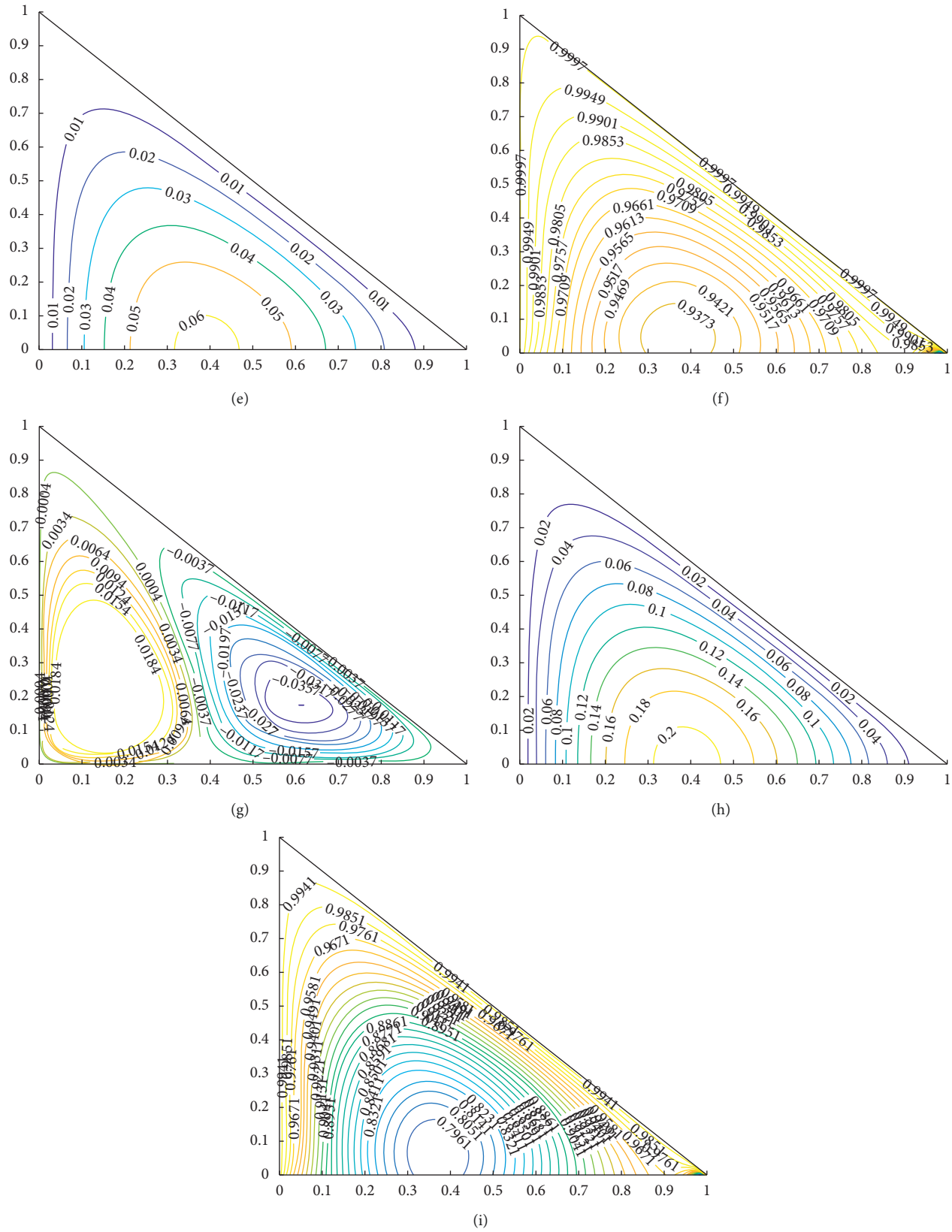

Figure 5: Stream function ψ, isotherms θ, and isoconcentrations ϕ for $R_a = 10$, $H_a = 1$, $L_e = 10$, $N_r = 0.1$, $N_b = N_t = 0.4$, and $F_k = 0.1$ for Figures (a)–(c), $F_k = 1$ for Figures (d)–(f), and $F_k = 3$ for Figures (g)–(i). (a) ψ. (b) θ. (c) ϕ. (d) ψ. (e) θ. (f) ϕ. (g) ψ. (h) θ. (i) ϕ.

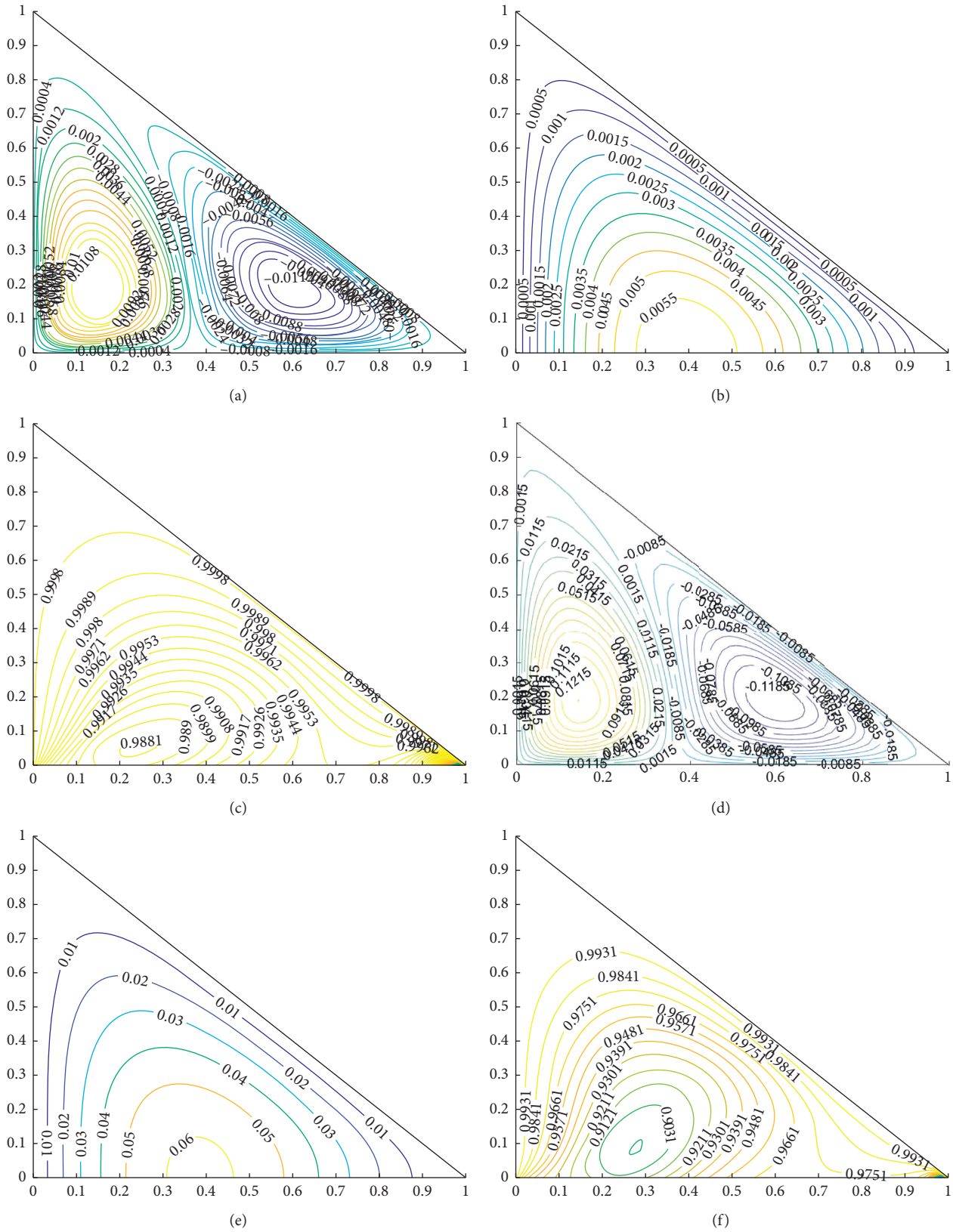

Figure 6: Continued.

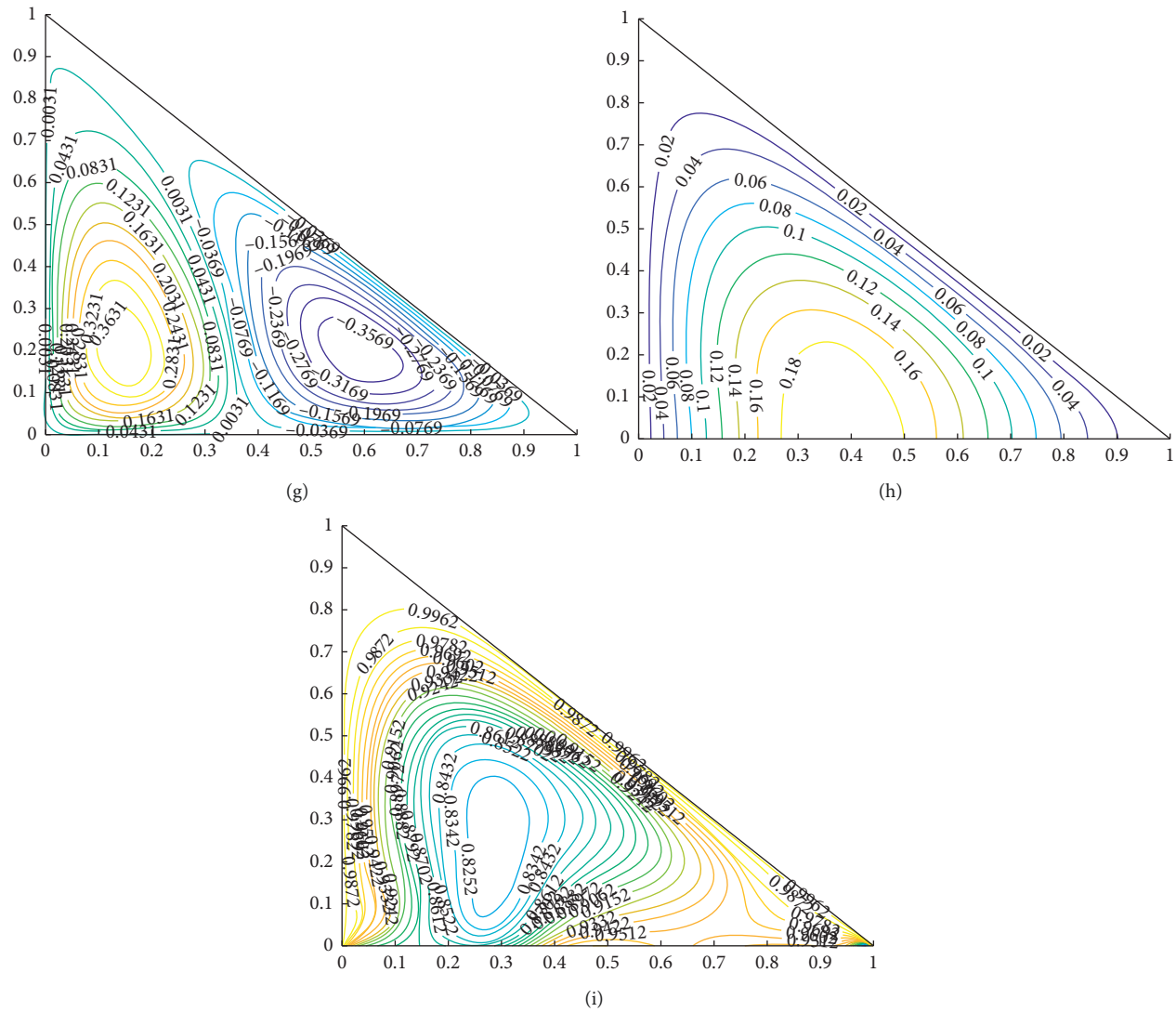

Figure 6: Stream function ψ, isotherms θ, and isoconcentrations ϕ for $R_a = 100$, $H_a = 1$, $L_e = 10$, $N_r = 0.1$, $N_b = N_t = 0.4$, and $F_k = 0.1$ for Figures (a)–(c), $F_k = 1$ for Figures (d)–(f), and $F_k = 3$ for Figures (g)–(i). (a) ψ. (b) θ. (c) ϕ. (d) ψ. (e) θ. (f) ϕ. (g) ψ. (h) θ. (i) ϕ.

and mass diffusivity. It is used to characterize fluid flows where there is simultaneous heat and mass transfer. The Lewis number is, therefore, a measure of the relative thermal and concentration boundary layer thicknesses. H_a is a dimensionless number known as Hartmann number, which gives a measure of the relative importance of drag forces resulting from magnetic induction and viscous forces in Hartmann flow and determines the velocity profile for such flow.

4.2. Effects of Frank-Kamenetskii and Rayleigh Numbers. The impact of the Frank-Kamenetskii number and the Rayleigh number on the evolution of streamlines, isotherms, and isoconcentrations is described in Figure 5 when $R_a = 10$ and $F_k = 0.1$ and in Figure 6 when $R_a = 100$ and $F_k = 0.1$, 1, and 3, respectively. From these figures, it is observed that in the case of streamlines, two opposite rotating vortices appear which are independent of the values of R_a and F_k. The values for other model parameters are $L_e = 10$, $N_b = 0.4$, $N_r = 0.1$, $N_t = 0.4$, and $H_a = 1$. A decrease in thermal and concentration boundary layer thicknesses is observed with the increase of R_a and F_k. The value of $\theta|_{\max}$ decreases with the rise in R_a, while it increases with the rise of F_k. The exothermic reaction produces more heat with growing value for F_k, hence accelerating the convection phenomenon within the cavity. For the smaller value of R_a, the isoconcentrations become concentrated towards the vertical wall where the heat is low. This concentration is due to the thermophoresis phenomenon since the nanoparticles flee towards cool regions from the hot regions. However, a vortex appears near a bottom wall for a higher value of R_a, which shifts towards the center of the cavity as the value F_k increases. Increase in R_a and F_k also intensifies the convective flow in the cavity accounting by the maximum $|\psi|$.

The monotonic effects of the Rayleigh number and the Frank-Kamenetskii number on heat transfer in terms of

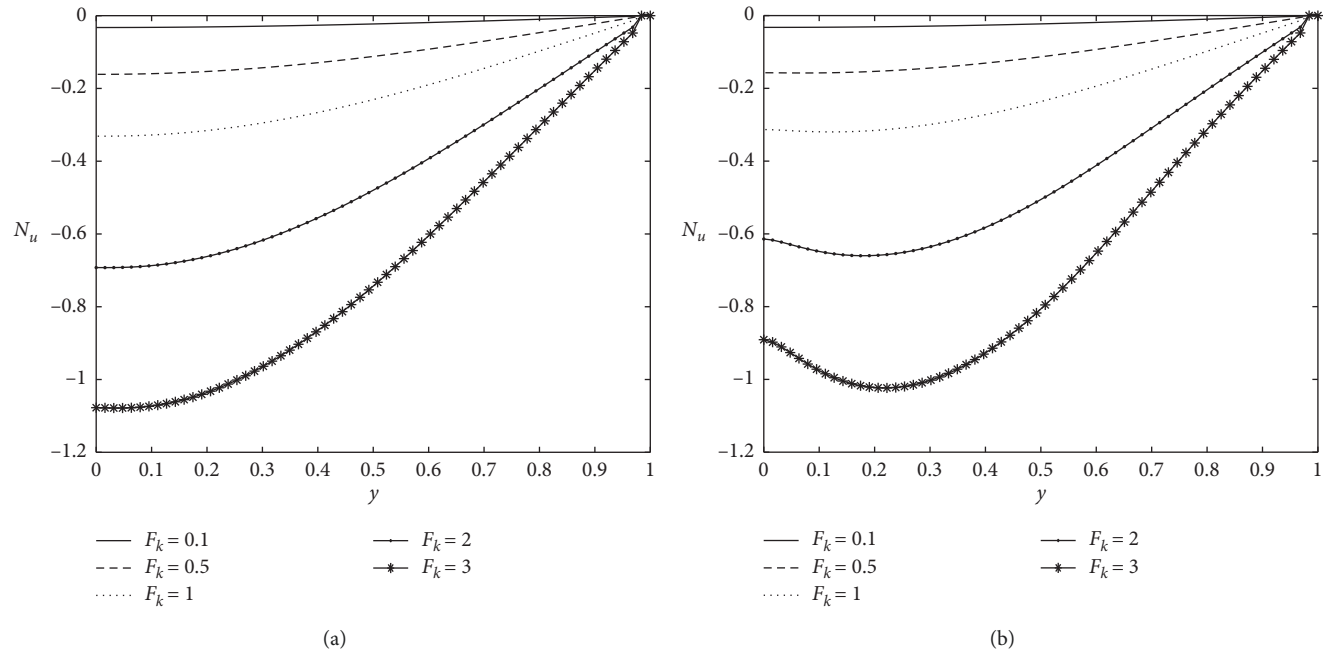

Figure 7: Variation of local Nusselt number when $L_e = 10$, $H_a = 1$, $N_b = 0.4$, $N_r = 0.1$, $N_t = 0.4$, and $R_a = 10$ (a) and $R_a = 100$ (b).

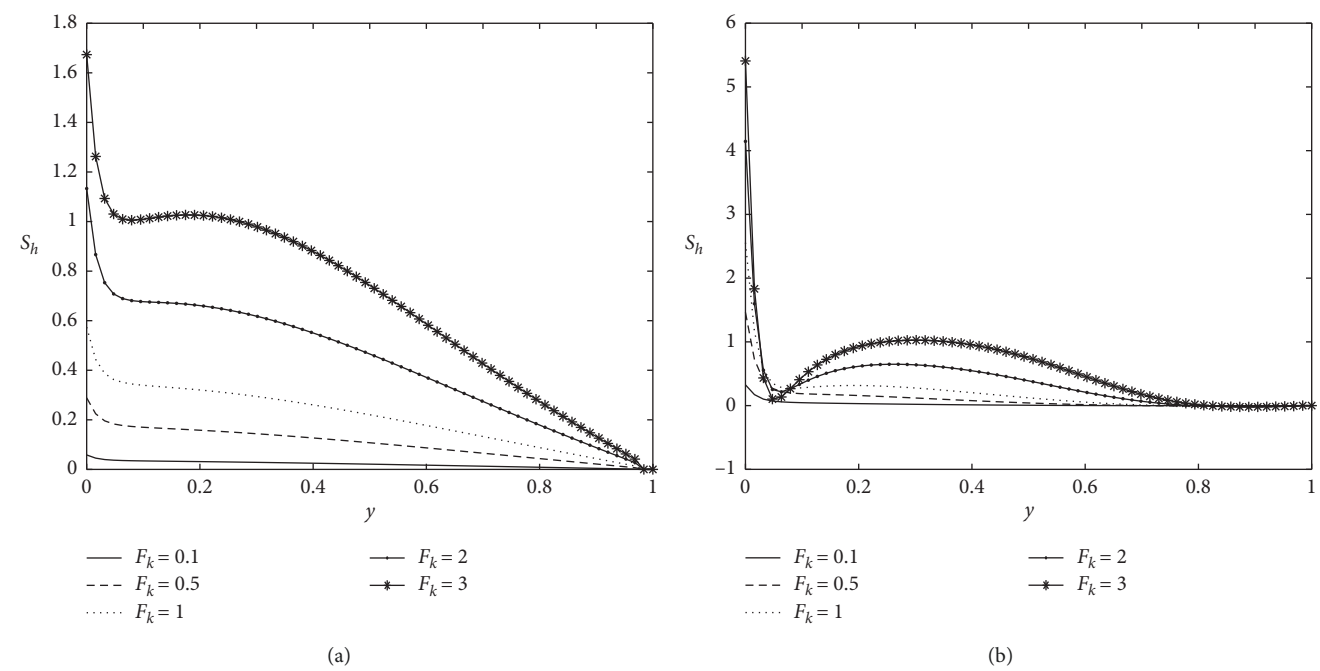

Figure 8: Variation of local Sherwood number when $L_e = 10$, $H_a = 1$, $N_b = 0.4$, $N_r = 0.1$, $N_t = 0.4$, and $R_a = 10$ (a) and $R_a = 100$ (b).

local Nusselt are depicted in Figure 7. An accretion of R_a with F_k leads to an increase in N_u due to an interaction of the thermal boundary layers close to the vertical walls. Similar results are obtained for local Sherwood number and plotted in Figure 8. For the higher value of R_a, the local Sherwood number decreases with $\overline{y}$, and particles become concentrated towards the vertical wall with a less significant effect of increasing Frank number F_k, resulting in a decrease in the nanoparticle volume fraction (Figure 9(b)). Figure 9 depicts that average Sherwood and Nusselt numbers decrease with the increasing value of R_a. This shows that the rate of heat and mass transfer decreases along the vertical wall, and the heat transfer is dominated by the conduction. Figure 10 is the mesh diagram for stream function ψ depicting the formation of two vortices. This pattern can also be viewed in Figures 5 and 6, where we noticed that the

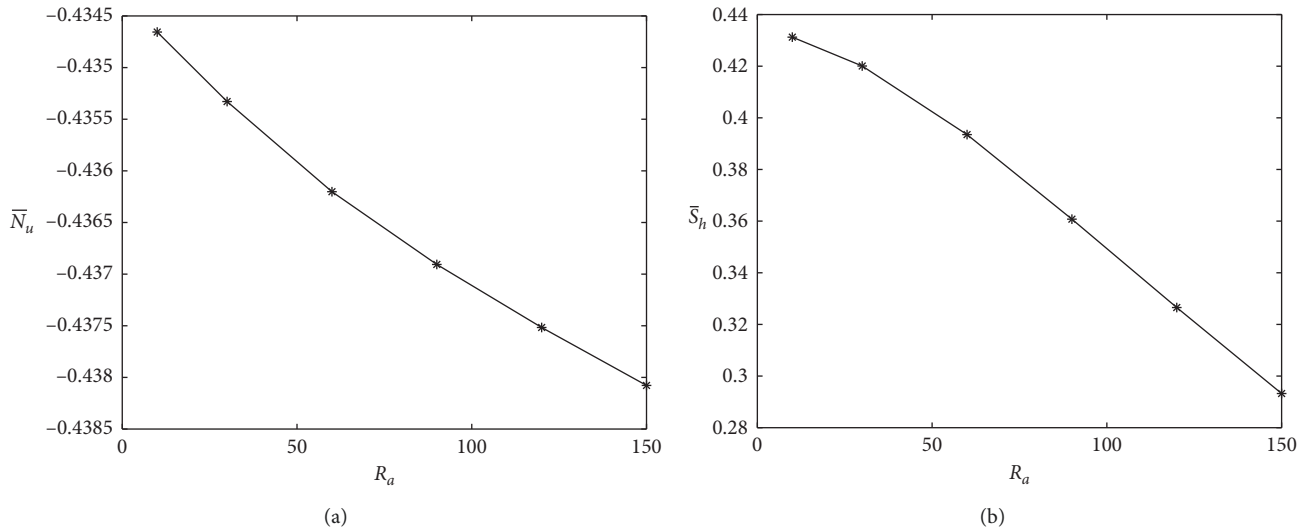

Figure 9: Variation of average Nusselt number (a) and average Sherwood number (b) at the vertical wall with varying R_a when $L_e = 10$, $H_a = 1$, $N_b = 0.4$, $N_r = 0.1$, and $N_t = 0.4$.

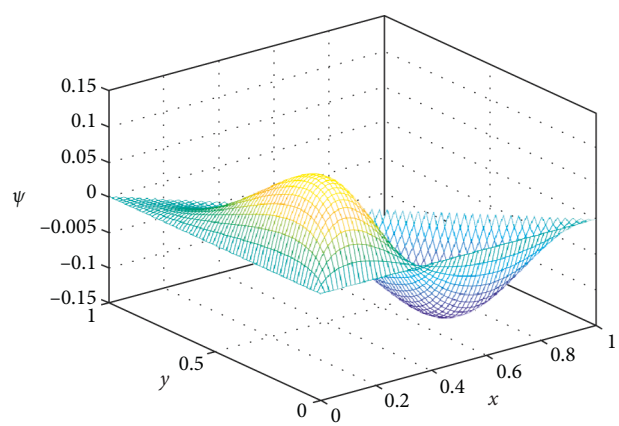

Figure 10: Mesh diagram for ψ.

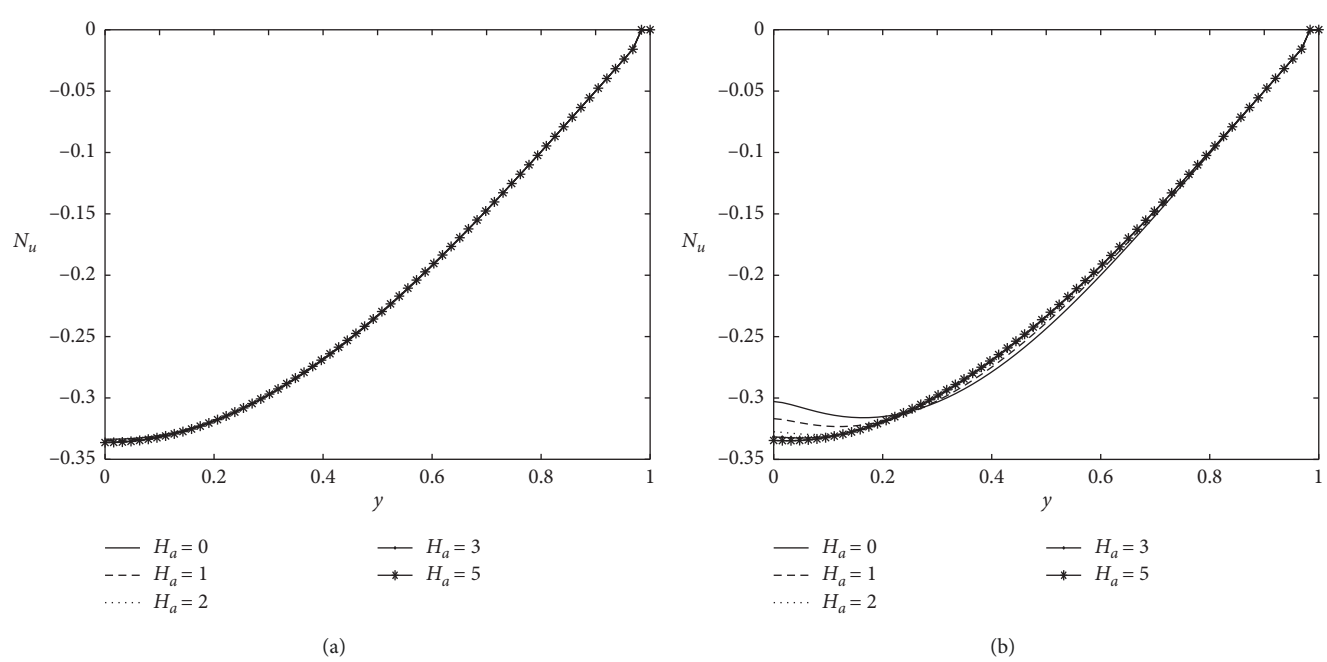

Figure 11: Variation of local Nusselt number when $L_e = 10$, $F_k = 1$, $N_b = 0.4$, $N_r = 0.1$, $N_t = 0.4$, and $R_a = 10$ (a) and $R_a = 100$ (b).

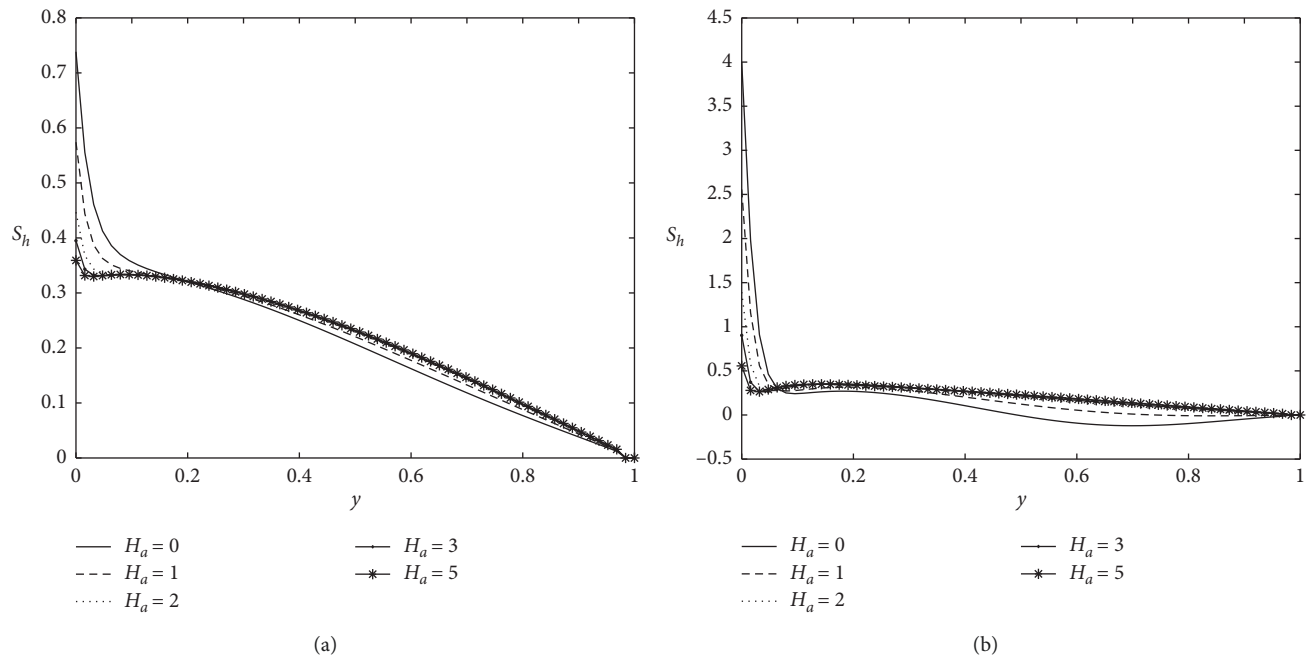

Figure 12: Variation of local Sherwood number when $L_e = 10$, $F_k = 1$, $N_b = 0.4$, $N_r = 0.1$, $N_t = 0.4$, and $R_a = 10$ (a) and $R_a = 100$ (b).

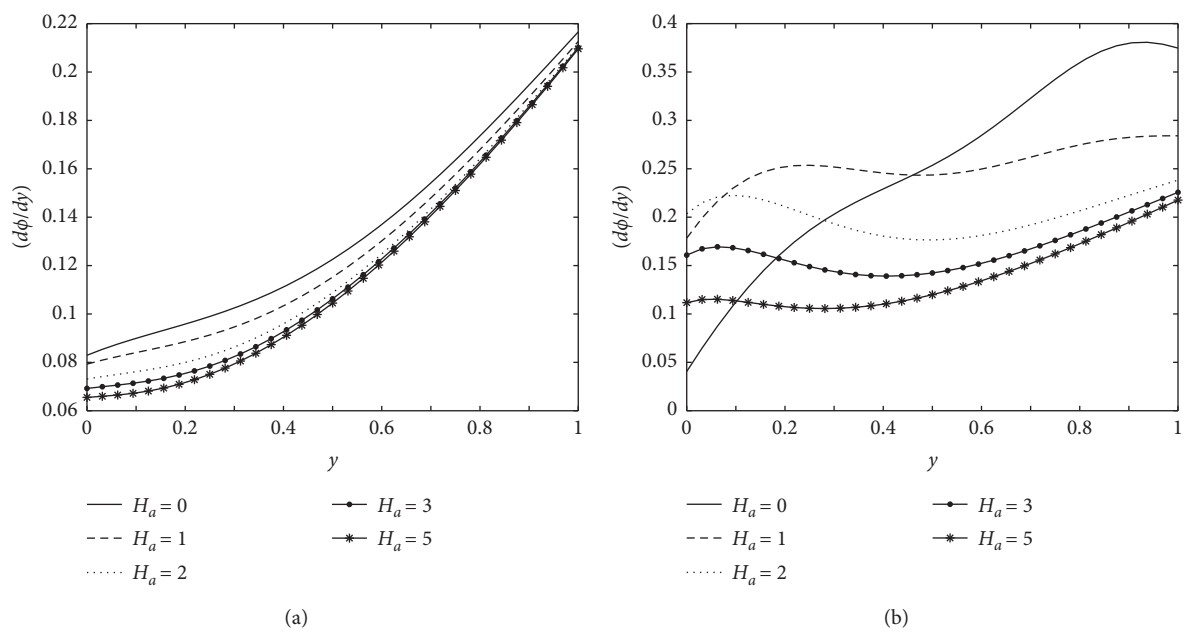

Figure 13: Gradients for nanoparticle concentration along $x = 0.5$ for different values of $L_e = 10$, $N_b = 0.4$, $N_r = 0.1$, $N_t = 0.4$, and $R_a = 10$ (a) and $R_a = 100$ (b).

nanofluid flows inside the triangular cavity which occurs in two major vortices. One vortex has a clockwise rotation in the left, while the second vortex has an anticlockwise rotation in the right half of the cavity. So, the Lorentz force increases the motion in the left half, and it decelerates the motion in the other half because the flow and the field act in the opposite direction. Since the applied magnetic field prevents the convection current, as a result, the average Nusselt number and Sherwood number decreases.

4.3. Effects of Hartmann and Rayleigh Numbers. In Figures 11 and 12, the effects of the Hartmann number on local Nusselt and Sherwood numbers with the variation of the Rayleigh number are plotted against the vertical wall of the cavity. For a weak flow ($R_a = 10$), the effect of Hartmann number on local Nusselt number is negligible, as shown in Figure 11(a). This is because when the Rayleigh number is small, the flow convection is insignificant and the heat transfer in the cavity is dominated by conduction. However,

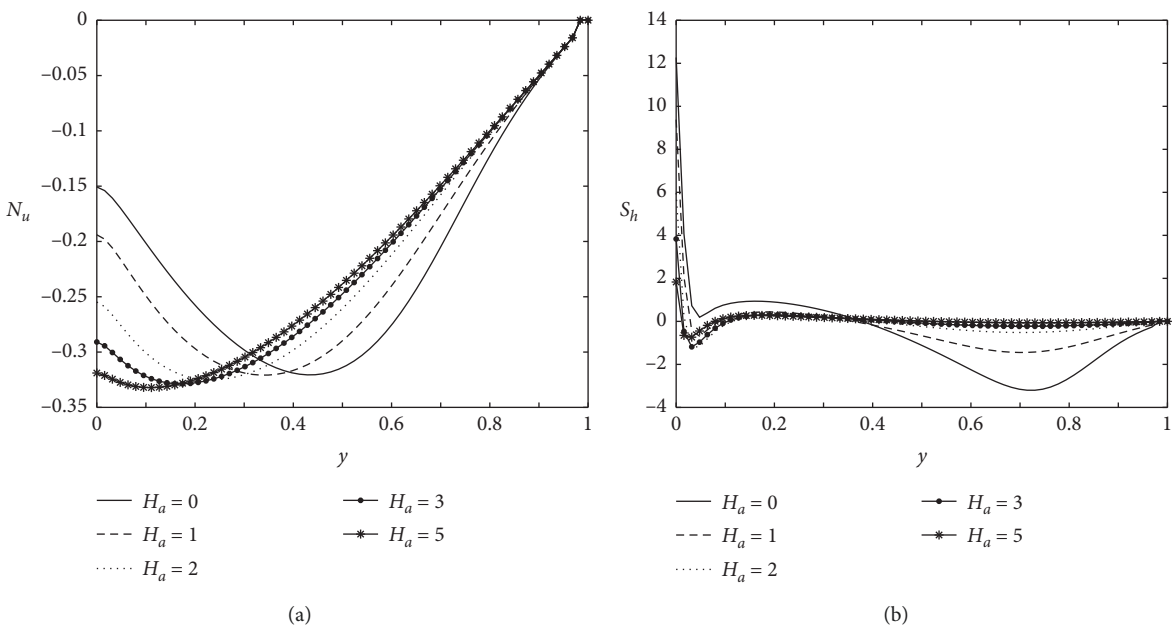

Figure 14: Variation of local Nusselt number (a) and local Sherwood number (b) when $L_e = 10$, $F_k = 1$, $N_b = 0.4$, $N_r = 0.01$, $N_t = 0.1$, and $R_a = 1000$.

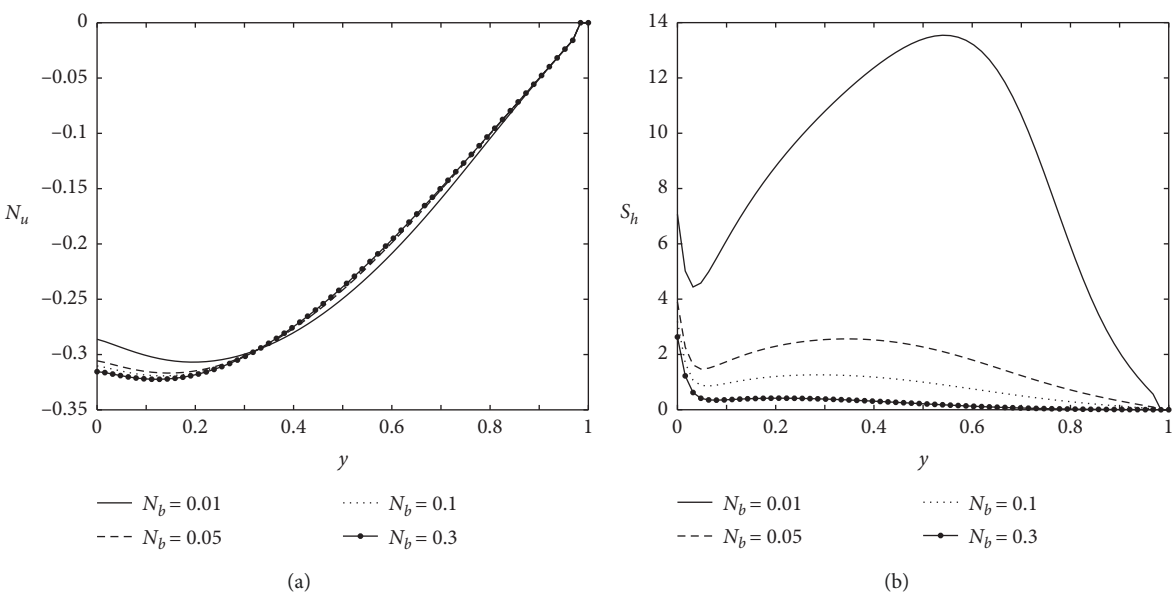

Figure 15: Deviations in local Nusselt number (a) local Sherwood number (b) when $L_e = 10$, $H_a = 1$, $F_k = 1$, $N_r = 0.1$, $N_t = 0.4$, and $R_a = 100$.

in the case of higher Rayleigh number, the N_u increases but depicts a small variation with H_a, as observed in Figure 11(b). Due to high Rayleigh number, the flow convection becomes stronger which in turn increases the heat transfer in the cavity. Similar to Figure 12(a), the effect of the Hartmann number on Sherwood number is minimal, and it decreases for both the lower and higher values of Rayleigh number, as shown in Figure 12(b).

It is also noted that a magnetic field with high intensity prevents the convection and may cause separation among nanoparticles. They are hence breaking the linearity of the gradient of nanoparticle concentration. To further check this aspect, we have plotted the concentration gradients $(\partial\phi/\partial y)$ along the center line ($x = 0.5$) of the enclosure for both cases of Rayleigh number, i.e., $R_a = 10$ and $R_a = 100$, for different values of Hartmann number, as displayed in Figure 13. For higher Rayleigh number, $R_a = 100$, the nanoparticles gather and start concentrating along the boundaries of the cavity away from the center, as can also be seen from Figure 6. Also, the deviations in gradients for nanoparticle concentration

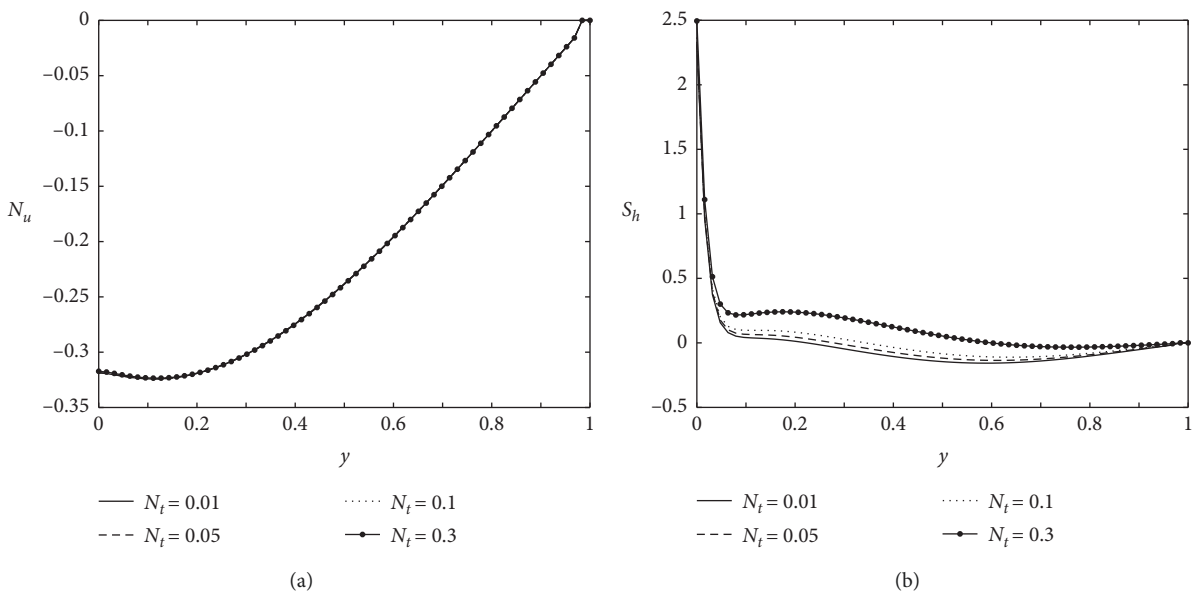

Figure 16: Deviations in local Nusselt number (a) local Sherwood number (b) when $L_e = 10$, $N_b = 0.4$, $N_r = 0.1$, and $R_a = 100$.

are nonlinear for a strong flow ($R_a = 100$), while for a weak flow ($R_a = 10$), $(\partial\phi/\partial y)$ is completely linear. Figure 14 shows the effects of the Hartmann number and Rayleigh number on local Nusselt and local Sherwood numbers. As the Hartmann number increases, the Nusselt number decreases. Similar is the trend observed for the Rayleigh number. The existence of the maximum and minimum points in the local Nusselt number profile corresponds to the presence of thermal plumes.

4.4. Effects of Brownian Diffusion and Thermophoresis Parameter. This section elaborates the effects of thermophoresis N_t and Brownian diffusion N_b parameters on the rate of heat and mass transfer which are observed along the vertical wall ($\overline{x} = 0$). Figure 15 illustrates the variation of local Nusselt and local Sherwood numbers for Brownian diffusion parameter. It is noticed from Figure 15(a) that the impact of N_b is quite less on the Nusselt number which distinctively agrees with the conclusions of Saghir and Mohamed [38]. However, the effect of these parameters on the mass transfer rate (Sherwood number) is quite noticeable. From Figure 15(b), it can be observed that as the particle size is smaller, the mass transfer is quite increased, while an increase in particle size diminishes the Brownian diffusion effect resulting in no change in the rate of mass transfer.

Figure 16 depicts the effects of thermophoresis parameter (N_t) on heat and mass transfer. Physically, the nanoparticles move from the hotter region towards the colder region due to the thermophoresis effect. From Figure 16(a), we found that the effect of N_t is almost negligible on the rate of heat transfer for the nanofluid flow inside the cavity filled with the porous medium. Once again the results reconfirm the conclusions of Saghir and Mohamed [38]. Figure 16(b) shows that the rate of mass transfer decreases along the vertical wall. But, the rate of the mass transfer becomes prominent with the growing N_t effect which leads to the homogeneous distribution of particles within a cavity.

5. Conclusions

A numerical analysis has been carried out to study the free convection within the triangular cavity filled with a porous medium saturated with nanofluids in the presence of magnetic field initiated by a chemical reaction influenced by Arrhenius kinetics. The finite difference method has been applied to solve the governing equations. The numerical results have been obtained and discussed for a wide range of physical parameters appearing in the problem. It is found that increasing the value of Rayleigh number decreases both the average Nusselt number and average Sherwood number. Moreover, the local Nusselt number increases with the variation of Frank-Kamenetskii number, Hartmann number, Brownian diffusion, and thermophoresis parameter for the increasing value of Rayleigh number. But, local Sherwood number decreases with the variation of Frank-Kamenetskii number, Hartmann number, Brownian diffusion, and thermophoresis parameter for the increasing value of Rayleigh number.

Appendix

Finite Difference Discretization

Based on the similar approach adopted in [31], equation (6) is discretized by using five-point stencil:

$$\left(1 + H_a^2\right)\left[\frac{\psi_{j,i+1}^{n+1} - 2\psi_{j,i}^{n+1} + \psi_{j,i-1}^{n+1}}{h^2}\right] + \left[\frac{\psi_{j+1,i}^{n+1} - 2\psi_{j,i}^{n+1} + \psi_{j-1,i}^{n+1}}{h^2}\right] = f_{j,i}^{n}, \tag{A.1}$$

where

$$f_{j,i}^{n} = -R_a \frac{\theta_{j,i+1}^{n} - \theta_{j,i-1}^{n}}{2h} + R_a N_r \frac{\phi_{j,i+1}^{n} - \phi_{j,i-1}^{n}}{2h}\left(1 + H_a^2\right)\psi_{j,i-1}^{n+1}$$
$$- 2\left(2 + H_a^2\right)\psi_{j,i}^{n+1} + \left(1 + H_a^2\right)\psi_{j,i+1}^{n+1} + \psi_{j-1,i}^{n+1} + \psi_{j+1,i}^{n+1} = h^2 f_{j,i}^{n}. \tag{A.2}$$

Similarly, equation (7) is discretized as follows:

$$\frac{\partial^2\theta^{n+1}}{\partial x^2} + \frac{\partial^2\theta^{n+1}}{\partial y^2} + \left(N_t\frac{\partial\theta^n}{\partial x} + N_b\frac{\partial\phi^n}{\partial x} - \frac{\partial\psi^{n+1}}{\partial y}\right)\frac{\partial\theta^{n+1}}{\partial x}$$
$$+ \left(N_t\frac{\partial\theta^n}{\partial y} + N_b\frac{\partial\phi^n}{\partial y} + \frac{\partial\psi^{n+1}}{\partial x}\right)\frac{\partial\theta^{n+1}}{\partial y} = -F_k e^{\theta^n},$$
$$\frac{\partial^2\theta^{n+1}}{\partial x^2} + \frac{\partial^2\theta^{n+1}}{\partial y^2} + a\frac{\partial\theta^{n+1}}{\partial x} + b\frac{\partial\theta^{n+1}}{\partial y} = -F_k e^{\theta^n}, \tag{A.3}$$

where

$$a = N_t\frac{\partial\theta^n}{\partial x} + N_b\frac{\partial\phi^n}{\partial x} - \frac{\partial\psi^{n+1}}{\partial y},$$
$$b = N_t\frac{\partial\theta^n}{\partial y} + N_b\frac{\partial\phi^n}{\partial y} + \frac{\partial\psi^{n+1}}{\partial x},$$
$$\left(1 - 0.5ha_{i-1,j}\right)\theta_{i-1,j}^{n+1} - 4\theta_{i,j}^{n+1} + \left(1 + 0.5ha_{i+1,j}\right)\theta_{i+1,j}^{n+1}$$
$$+ \left(1 - 0.5hb_{i,j-1}\right)\theta_{i,j-1} + \left(1 + 0.5hb_{i,j+1}\right)\theta_{i,j+1} = -h^2 F_k \exp\left(\theta_{i,j}\right), \tag{A.4}$$

where

$$a_{i,j} = Nt\frac{\theta_{i+1,j}^{n} - \theta_{i,j}^{n}}{h} + Nb\frac{\phi_{i+1,j}^{n} - \phi_{i,j}^{n}}{h} - \frac{\psi_{i,j+1}^{n+1} - \psi_{i,j}^{n+1}}{h},$$
$$b_{i,j} = Nt\frac{\theta_{i,j+1}^{n} - \theta_{i,j}^{n}}{h} + Nb\frac{\phi_{i,j+1}^{n} - \phi_{i,j}^{n}}{h} + \frac{\psi_{i+1,j}^{n+1} - \psi_{i,j}^{n+1}}{h}. \tag{A.5}$$

The Neumann boundary condition for temperature equation (11) is discretized as

$$\frac{\theta_{i,1} - \theta_{i,0}}{h} = 0,$$
$$\theta_{i,0} = \theta_{i,1}, \quad \forall i. \tag{A.6}$$

Also, equation (8) is discretized as follows:

$$\nabla^2\phi^{n+1} - L_e\left(\frac{\partial\psi^{n+1}}{\partial Y}\frac{\partial\phi^{n+1}}{\partial X} - \frac{\partial\psi^{n+1}}{\partial X}\frac{\partial\phi^{n+1}}{\partial Y}\right) = -\frac{N_t}{N_b}\nabla^2\theta^{n+1},$$
$$\nabla^2\phi^{n+1} + c\frac{\partial\phi^{n+1}}{\partial X} + d\frac{\partial\phi^{n+1}}{\partial Y} = g, \tag{A.7}$$

where

$$c = -L_e\frac{\partial\psi^{n+1}}{\partial Y},$$
$$d = L_e\frac{\partial\psi^{n+1}}{\partial X}, \tag{A.8}$$
$$g = -\frac{N_t}{N_b}\nabla^2\theta^{n+1}.$$

The discretized form of the aforementioned equation is

$$\left(1 - 0.5hc_{i-1,j}\right)\phi_{i-1,j}^{n+1} - 4\phi_{i,j}^{n+1} + \left(1 + 0.5hc_{i+1,j}\right)\phi_{i+1,j}$$
$$+ \left(1 - 0.5hd_{i,j-1}\right)\phi_{i,j-1}^{n+1} + \left(1 + 0.5hd_{i,j+1}\right)\phi_{i,j+1}^{n+1} = h^2 g_{i,j}^{n+1}, \tag{A.9}$$

where

$$c_{i,j} = -L_e\frac{\psi_{i,j+1}^{n+1} - \psi_{i,j}^{n+1}}{h},$$
$$d_{i,j} = L_e\frac{\psi_{i+1,j}^{n+1} - \psi_{i,j}^{n+1}}{h},$$
$$g_{i,j} = -\frac{N_t}{N_b}\left(\frac{\theta_{i-1,j}^{n+1} - 2\theta_{i,j}^{n+1} + \theta_{i+1,j}^{n+1}}{h^2} + \frac{\theta_{i,j+1}^{n+1} - 2\theta_{i,j}^{n+1} + \theta_{i,j-1}^{n+1}}{h^2}\right). \tag{A.10}$$

Nomenclature

a:	Concentration of the reactant A
B:	Magnetic field strength T
C:	Nanoparticle volume fraction
C_0:	Reference nanoparticle volume fraction
D_B:	Brownian diffusion coefficient $m^2 \cdot s^{-1}$
D_T:	Thermopheric diffusion coefficient $m^2 \cdot s^{-1}$
E:	Activation energy
F_k:	Frank-Kamenetskii number
g:	Gravitational acceleration $m^2 \cdot s^{-1}$
H:	Height of the triangular cavity m
H_a:	Magnetic field parameter
K:	Permeability of the porous medium md^{-1}
k_0:	Pre-exponential factor
k_m:	Effective thermal conductivity of the porous medium
L_e:	Lewis number
N_b:	Brownian motion parameter
N_r:	Buoyancy-ratio parameter
N_t:	Thermophoresis parameter
N_u:	Local Nusselt number
$\overline{N_u}$:	Average Nusselt number
P^*:	Pressure
P:	Dimensionless pressure
R:	Fluid constant
R_a:	Rayleigh number
Q:	Exothermicity factor
T:	Nanofluid temperature
T_0:	Reference value for temperature

$\overline{u}$, $\overline{v}$: Velocity components in the $\overline{x}$, $\overline{y}$ directions $m \cdot s^{-1}$
V: Nanofluid velocity
$\overline{x}$, $\overline{y}$: Dimensional coordinates in the direction of bottom and vertical wall m (B,01) α_m thermal diffusivity of the porous medium $m^2 \cdot s^{-1}$
β: Thermal expansion coefficient K^{-1}
ε: Porosity
μ: Viscosity of the fluid $kg \cdot m^{-1} \cdot s^{-1}$
ψ: Dimensionless stream function
ψ: Dimensionless nanoparticle volume fraction
ρ: Fluid density $kg \cdot m^{-3}$
ρ_{f_0}: Reference density of the nanofluid
ρ_p: Nanoparticle mass density
$(\rho c)_f$: Heat capacity of the nanofluid $J \cdot K^{-1} \cdot m^{-3}$
$(\rho c)_m$: Effective heat capacity of the porous medium
$(\rho c)_p$: Heat capacity of the nanoparticle material
θ: Dimensionless temperature.

Data Availability

All the data are included in the article. If there is a further demand for data, the author can provide depending on their availability.

Conflicts of Interest

The author declares that there are no conflicts of interest.

References

[1] I. Pop and D. Ingham, *Convective Heat Transfer: Mathematical and Computational Modeling of Viscous Fluids and Porous Media*, Elsevier Science & Technology Books, Amsterdam, Netherlands, 2001.

[2] J. Bear, *Modeling Phenomena of Flow and Transport in Porous Media*, vol. 31, Springer, Berlin, Germany, 2018.

[3] A. C. Baytas and I. Pop, "Free convection in oblique enclosures filled with a porous medium," *International Journal of Heat and Mass Transfer*, vol. 42, no. 6, pp. 1047–1057, 1999.

[4] Q. Sun and I. Pop, "Free convection in a triangle cavity filled with a porous medium saturated with nanofluids with flush mounted heater on the wall," *International Journal of Thermal Sciences*, vol. 50, no. 11, pp. 2141–2153, 2011.

[5] M. Izadi, N. M. Maleki, I. Pop, and S. A. M. Mehryan, "Natural convection of a hybrid nanofluid subjected to non-uniform magnetic field within porous medium including circular heater," *International Journal of Numerical Methods for Heat & Fluid Flow*, vol. 29, no. 4, pp. 1211–1231, 2019.

[6] F. Arpino, A. Carotenuto, M. Ciccolella, G. Cortellessa, N. Massarotti, and A. Mauro, "Transient natural convection in partially porous vertical annuli," *International Journal of Heat and Technology*, vol. 34, no. 2, pp. S512–S518, 2016.

[7] F. Arpino, N. Massarotti, and A. Mauro, "A stable explicit fractional step procedure for the solution of heat and fluid flow through interfaces between saturated porous media and free fluids in presence of high source terms," *International Journal for Numerical Methods in Engineering*, vol. 83, no. 6, pp. 671–692, 2010.

[8] F. Arpino, N. Massarotti, and A. Mauro, "Efficient three-dimensional fem based algorithm for the solution of convection in partly porous domains," *International Journal of Heat and Mass Transfer*, vol. 54, no. 21-22, pp. 4495–4506, 2011.

[9] N. Massarotti, M. Ciccolella, G. Cortellessa, and A. Mauro, "New benchmark solutions for transient natural convection in partially porous annuli," *International Journal of Numerical Methods for Heat & Fluid Flow*, vol. 26, no. 3/4, pp. 1187–1225, 2016.

[10] M. A. Sheremet and I. Pop, "Free convection in a triangular cavity filled with a porous medium saturated by a nanofluid buongiorno's mathematical model," *International Journal of Numerical Methods for Heat and Fluid Flow*, vol. 25, no. 5, pp. 1138–1161, 2014.

[11] J. Buongiorno, "Convective transport in nanofluids," *Journal of Heat Transfer*, vol. 128, no. 3, pp. 240–250, 2006.

[12] H. F. Oztop and E. Abu-Nada, "Numerical study of natural convection in partially heated rectangular enclosures filled with nanofluids," *International Journal of Heat and Fluid Flow*, vol. 29, no. 5, pp. 1326–1336, 2008.

[13] S. U. S. Choi, "Enhancing thermal conductivity of fluids with nanoparticles," *Development and Applications of Non-newtonian Flows*, vol. 231, no. 66, pp. 99–105, 1995.

[14] A. V. Kuznetsov and D. A. Nield, "The cheng-minkowycz problem for natural convective boundary layer flow in a porous medium saturated by a nanofluid: a revised model," *International Journal of Heat and Mass Transfer*, vol. 65, pp. 682–685, 2013.

[15] D. A. Nield and A. V. Kuznetsov, "Thermal instability in a porous medium layer saturated by a nanofluid," *International Journal of Heat and Mass Transfer*, vol. 52, no. 25-26, pp. 5796–5801, 2009.

[16] D. A. Nield and A. Bejan, *Convection in Porous Media*, Springer, New York, NY, USA, 4th edition, 2013.

[17] W. YuS, K. Das, S. U. S. Choi, and T. Pradeep, *Nanofluids: Science and Technology*, Wiley, Hoboken, NJ, USA, 2007.

[18] A. J. Chamkha, "Hydromagnetic combined convection flow in a vertical lid-driven cavity with internal heat generation or absorption," *Numerical Heat Transfer, Part A: Applications*, vol. 41, no. 5, pp. 529–546, 2002.

[19] A. Malleswaran and S. Sivasankaran, "A numerical simulation on mhd mixed convection in a lid-driven cavity with corner heaters," *Journal of Applied Fluid Mechanics*, vol. 9, pp. 311–319, 2016.

[20] M. A. AlimM, M. Rahman, and M. M. A. Sarker, "Numerical study on the conjugate effect of joule heating and magnetohydrodynamics mixed convection in an obstructed lid-driven square cavity," *International Communications in Heat and Mass Transfer*, vol. 37, pp. 524–534, 2010.

[21] M. M. Rahman, I. Pop, and M. Z. Saghir, "Steady free convection flow within a titled nanofluid saturated porous cavity in the presence of a sloping magnetic field energized by an exothermic chemical reaction administered by Arrhenius kinetics," *International Journal of Heat and Mass Transfer*, vol. 129, pp. 198–211, 2019.

[22] J. H. Merkin and M. A. Chaudhary, "Free-convection boundary layers on vertical surfaces driven by an exothermic surface reaction," *The Quarterly Journal of Mechanics and Applied Mathematics*, vol. 47, no. 3, pp. 405–428, 1994.

[23] T. Mahmood and J. H. Merkin, "The convective boundary-layer flow in a reacting surface in a porous medium," *Transport in Porous Media*, vol. 32, no. 3, pp. 285–298, 1998.

[24] H. Ikeda, P. A. Libby, F. A. Williams, and J. I. Sato, "Catalytic combustion of hydrogen-air mixtures in stagnation flows," *Combustion and Flame*, vol. 93, no. 1-2, pp. 138–148, 1993.

[25] B. F. Gray and J. H. Merkin, "Thermal explosion: escape times in the uniform temperature approximation. Part I: Effects of parameter perturbations," *Journal of the Chemical Society, Faraday Transactions*, vol. 86, no. 4, pp. 597–601, 1990.

[26] B. F. Gray and J. H. Merkin, "Thermal explosion: escape times in the uniform temperature approximation. Part II: perturbations of critical initial conditions," *International Journal of Mathematical Engineering with Industrial Applications*, vol. 4, no. 13–26, 1993.

[27] J. H. Merkin and I. Pop, "Stagnation point flow past a stretching/shrinking sheet driven by arrhenius kinetics," *Applied Mathematics and Computation*, vol. 337, pp. 583–590, 2018.

[28] A. Lazarovici, V. Volpert, and J. H. Merkin, "Steady states, oscillations and heat explosion in a combustion problem with convection," *European Journal of Mechanics–B/Fluids*, vol. 24, no. 2, pp. 189–203, 2005.

[29] M. M. Rahman, "Combined effects of internal heat generation and higher order chemical reaction on the non-darcian forced convective flow of a viscous incompressible fluid with variable viscosity and thermal conductivity over a stretching surface embedded in a porous med," *The Canadian Journal of Chemical Engineering*, vol. 90, no. 6, pp. 1632–1645, 2012.

[30] S. S. S. CardosoT, Y. Liu, A. N. Campbell, and A. N. Hayhurst, "Effects of natural convection on thermal explosion in a closed vessel," *Chemistry, Physics, Chemical Engineering*, vol. 10, pp. 5521–5530, 2008.

[31] M. Raees Ul Haq, H. Xu, and L. Zhao, "Study of electrokinetic effects for heat transfer in microchannel with sinusoidal thermal boundary conditions," *International Journal of Numerical Methods for Heat & Fluid Flow*, vol. 9, 2019.

[32] K. L. Walker and G. M. Homsy, "Convection in a porous cavity," *Journal of Fluid Mechanics*, vol. 87, pp. 447–474, 1978.

[33] A. Bejan, "On the boundary layer regime in a vertical enclosure filled with a porous medium," *Letters in Heat and Mass Transfer*, vol. 6, no. 2, pp. 93–102, 1979.

[34] C. Beckermann, R. Viskanta, and S. Ramadhyani, "A numerical study of non-darcian natural convection in a vertical enclosure filled with a porous medium," *Numerical Heat Transfer, Part B: Fundamentals*, vol. 10, no. 6, pp. 557–570, 1986.

[35] R. J. Gross, M. R. Bear, and C. E. Hickox, "The application of flux-corrected transport (FCT) to high Rayleigh number natural convection in a porous medium," in *Proceedings of the 8th International Heat Transfer Conference*, San Francisco, CA, USA, 1986.

[36] E. RamosS, L. Moya, and M. Sen, "Numerical study of natural convection in a tilted rectangular porous m aterial," *International Journal of Heat and Mass Transfer*, vol. 30, pp. 741–756, 1987.

[37] D. M. Manole and J. L. Lage, "Numerical benchmark results for natural convection in a porous medium cavity," in *ASME Conference*, vol. vol. 216 of Heat and Mass Transfer in Porous Media, pp. 55–60, Koln Messe, Cologne, Germany, June 1992.

[38] M. Z. Saghir and A. Mohamed, "Effectiveness in incorporating Brownian and thermophoresis effects in modelling convective flow of water-Al_2O_3 nanoparticles," *International Journal of Numerical Methods for Heat & Fluid Flow*, vol. 28, no. 1, pp. 47–63, 2018.